crystals

MDPI

Review

Characterization of Defects in GaN: Optical and Magnetic Resonance Techniques

Jaime A. Freitas, Jr. *, James C. Culbertson and Evan R. Glaser

Naval Research Laboratory, Washington, DC 20375, USA
* Correspondence: jaime.freitas@nrl.navy.mil

Abstract: GaN and its alloys with InN and AlN are of technological importance for a variety of optical, electronic, and optoelectronic devices due to its high thermal conductivity, wide band gap, high breakdown voltage and high saturation velocity. GaN-based devices now provide superior performance for a variety of high power, high frequency, high temperature, and optical applications. The major roadblock for the full realization of Nitride semiconductor potential is still the availability of affordable large-area and high-quality native substrates with controlled electrical properties. Despite the impressive accomplishments recently achieved by techniques such as hydride vapor phase epitaxy and ammonothermal for GaN growth, much more must be attained before establishing a fully satisfactory bulk growth method for this material. Recent results suggest that ammonothermal GaN wafers can be successfully used as seeds to grow thick freestanding GaN wafers by hydride vapor phase epitaxy. A brief review of defect-sensitive optical and paramagnetic spectroscopy techniques employed to evaluate structural, optical, and electronic properties of the state-of-the-art bulk and thick-film (quasi-bulk) Nitride substrates and homoepitaxial films is presented. Defects control the performance of devices and feeding back knowledge of defects to growth efforts is key to advancing technology.

Keywords: GaN; HVPE; ammonothermal; epitaxial; Raman scattering; photoluminescence; magnetic resonance

Citation: Freitas, J.A., Jr.; Culbertson, J.C.; Glaser, E.R. Characterization of Defects in GaN: Optical and Magnetic Resonance Techniques. *Crystals* **2022**, *12*, 1294. https://doi.org/10.3390/cryst12091294

Academic Editor: Evgeniy N. Mokhov

Received: 15 August 2022
Accepted: 4 September 2022
Published: 14 September 2022

1. Introduction

Gallium nitride (GaN) is a semiconductor that has an unusual combination of extreme values of fundamental physical and chemical properties. Its unique characteristics have made possible the fabrication of a variety of optoelectronic and electronic devices capable of performing at extreme operation conditions of current, voltage, temperature, and in harsh environments. The direct and wide bandgap (3.4 eV at room temperature) of GaN results in a low intrinsic carrier density that leads to low leakage and dark currents, crucial requirements for photo-detectors and high-temperature electronic applications. Despite the relatively large carrier effective masses, which lead to lower carrier mobilities, the high electron saturation velocity and high breakdown field make possible the fabrication of high frequency electronic devices. In addition, its relatively high thermal conductivity opens the possibility to realize a number of high-power device applications.

Presently, the major hurdle for full realization of the potential of GaN devices is the lack of commercial availability of large area, high-crystalline quality native substrates with full control of electrical properties. Low pressure Li- and Na-based solution growth methods only produced platelets and needle shaped crystals [1,2]. The high nitrogen pressure solution technique only yielded hexagonal platelets or needles from the gallium melt with 1 at% nitrogen at temperatures up to 1700 °C and nitrogen pressure of 20 kbar [3]. Also, GaN decomposes before melting and, thus, requires extremely high pressure to prevent premature decomposition [4]. In addition, GaN does not sublime, precluding the use of vapor transport techniques for bulk GaN growth.

For many decades the lack of native substrates for homoepitaxial growth compelled material scientists to develop a deeper understanding of the nucleation process and to optimize the properties of nucleation/buffer layers, which mitigate problems related to heteroepitaxial growth [5,6]. As a result, the deposition of device-quality films on foreign substrates (e.g., sapphire, Si, SiC, etc.) was accomplished. The resulting optimized heteroepitaxial films have relatively smooth surfaces and improved crystalline quality [7], and have lower intrinsic n-type background carrier concentration, which allows carrier type control. Such templates have been successfully used to fabricate a number of commercial optoelectronic and electronic devices [8]. Despite these remarkable achievements, the properties of thin heteroepitaxial nitride films still seriously limit the performance of devices demanding higher material yields, such as solid state lighting (which requires high quantum efficiency light emitting diodes), laser diodes, and high-frequency/high-power electronic devices, such as field effect and high electron mobility transistors. The high growth temperatures usually required to produce wide bandgap materials exacerbates fundamental material problems such as residual stress, differences in thermal expansion coefficients, low energy defect formation, and impurity incorporation. In addition, doping activation and self-compensation are difficult to control at the typically high deposition temperatures. Furthermore, the high concentration of dislocations, resulting mostly from lattice constant mismatch, typically on the order of 10^8 to $10^{10}/cm^2$, must be reduced to improve device performance. Overcoming these limitations will require the use of native substrates to grow electronic grade homoepitaxial layers.

Presently, Hydride Vapor Phase Epitaxy (HVPE) and Ammonothermal bulk growth are the only two methods that have successfully demonstrated the manufacturing of GaN boules. The first, a non-equilibrium process, only reproduces the starting substrate dimensions, while the latter, an equilibrium process, allows increasing boule dimensions under controlled growth conditions. In this work, we illustrate how several defect-sensitive optical and paramagnetic spectroscopy techniques can be used to assist the optimization procedures at various stages of growth.

2. Experimental Methods

Raman scattering (RS) is the most commonly used technique to study vibrational phenomena in solids. This well-established non-invasive/non-destructive technique used to identify crystal structure and verify crystalline quality is based on the observation of vibrational modes and their polarization selection rules. The magnitudes of the incident and scattered radiation wavevectors are much smaller than that of a general vector in the Brillouin Zone (BZ). Hence, in order to conserve the wavevector the created (Stokes) or annihilated (anti-Stokes) phonon must have a wavevector of magnitude near zero, i.e., near the center of the BZ; or Γ-point. Thus, the first order RS can investigate only phonons near the center of the BZ. Phonons with larger wavevectors may be observed in second order (two phonon) Raman spectra. Micro-Raman (μ-RS), which uses a probing laser spot size $\leq$1 μm, allows the evaluation of sample morphology, grain boundary orientation, strain, and impurity distribution. For the case of wurtzite GaN group theory predicts eight Brillouin zone-center optical vibrational modes, namely $1A_1$(TO), $1A_1$(LO), $2B_1$, $1E_1$(TO), $1E_1$(LO), and $2E_2$. The two $2B_1$ modes are optically inactive, but all the allowed optical modes have been observed by RS [9]. It is useful to note that the energy position of the E_2 mode is very sensitive to strain and the energy positions of the A_1(LO) and E_1(LO) modes are very sensitive to free-carrier concentration.

Photoluminescence (PL) is one of the most widely used spectroscopic techniques to characterize semiconductor materials because it is suitable, sensitive, non-destructive, and relatively inexpensive to implement. There are very few constraints on material preparation and a broad scope of phenomena, such as excitation processes, recombination mechanisms, point- and extended-defects, can be investigated. Semiconductor materials characterization by PL spectroscopy requires the measurement and interpretation of the spectral distribution of recombination radiation emitted by the sample. Electrons and holes

that are optically excited across the forbidden energy gap usually become localized or bound at an impurity or defect prior to recombining. The identity of these localization centers can often be determined from the PL spectrum. Relatively sharp lines are observed in the near-band edge spectral region, which arise from the recombination of electron-hole pairs that form bound excitons (BE) at impurity sites, or free-to-bound (FB) transitions due to recombination of free electrons (holes) with holes (electrons) bound at neutral acceptors (donors). Much broader emission bands, at lower energies, arise from the recombination of carriers localized at deep centers. Qualitative information about crystal quality can be inferred from the quantum efficiency and line widths of the near band-edge PL spectra, and impurities can sometimes be identified on the basis of the binding energies inferred from the spectral positions (energies) of the BE or FB transitions. One of the facts that make PL spectroscopy extremely useful is its application during all phases of the development of a new material system or growth technique. Typically, broad PL spectra that convey only the most qualitative information are obtained from poor quality semiconductor materials while sharper spectral features, which provide more specific information, will evolve as material quality improves. This has certainly been true of the PL characterization of the GaN films and bulk substrates that will be briefly reviewed in this manuscript.

Magnetic resonance techniques have been widely used to characterize defects in GaN over the last 30 years. In particular, the interaction of the electronic spin and an applied dc magnetic field splits the ground and excited states associated with point (such as dopants and transition metals) and lattice defects (such as vacancies, interstitials, and anti-sites) into one or more levels. Absorption of fixed energy microwaves at resonance conditions (described below) can induce transitions between these levels and can be detected, in principle, by spin resonance techniques such as electron paramagnetic resonance (EPR) and optically-detected magnetic resonance (ODMR). EPR gives important information on the ground state defect properties like their unique Zeeman splitting 'g-factors' and possible chemical identification thru resolved electron-nuclear hyperfine (HF) structure. In addition, with an appropriate standard, the EPR technique provides a quantitative measure of the defect densities in various GaN materials. ODMR, a complementary magnetic resonance technique, combines the attributes of EPR with the sensitivity and selectivity of PL. Though not quantitative like EPR, the ODMR technique provides information on the magnetic properties of the optically excited donor and acceptor states that participate directly (or sometimes indirectly) in radiative recombination processes.

2.1. Technical Approach

μ-RS measurements were performed using a single-mode 488 nm solid state laser, which was made coaxial with the detection axis using the beam-splitter part of a Volume-Bragg-Grating filter set from Optigrate. These filters allow Stokes and anti-Stokes Raman measurements closer than 10 cm^{-1} to the laser. A 50x microscope objective (NA = 0.65) was used to both focus the incident light into a small spot (~0.4 μm) and collect the scattered light, which then was dispersed in a half-meter Acton SP-2500 single-spectrometer and detected using a Princeton Instruments CCD array (Spec-10:400BR back-thinned, deep-depleted). All μ-RS measurements shown here were acquired in a back-scattering geometry $z(yy)\bar{z}$. The axis of the incident 488 nm light was normal to the sample surfaces and light back-scattered parallel to the incident beam was collected and measured.

The low temperature PL spectra described here were obtained with the samples contained in a liquid helium cryostat, which provides temperatures ranging from 1.5 to 330 K. Most of the spectra were obtained in CW mode with excitation provided by a HeCd laser (325 nm) or argon ion laser (351 nm). These excitation photon energies are above the 3.54 eV low temperature direct band gap of hexagonal wurtzite GaN. Calibrated neutral density filters were used to maintain the incident power within desired limits to prevent sample heating, and to allow the observation of recombination processes with different lifetimes. The emitted light was dispersed by an 1800 grooves/mm 0.85-m double-

grating spectrometer and detected by a UV-sensitive GaAs photomultiplier coupled to a computer-controlled photon counter system.

The EPR spectra were acquired using a commercial (E-300) Bruker spectrometer operating at a frequency of 9.51 GHz. The spectrometer was equipped with a liquid helium flow system that allowed for temperature control from 4.2–300 K. Typical microwave powers of 2–6 mW with 1–2 G modulation amplitude and 100 kHz field modulation were employed for these experiments. The g-values were calibrated with use of a DPPH (2,2-diphenyl-1-picrylhydrazyl) standard while a P-doped Si sample was used as a standard to obtain the density of spins associated with the EPR signals. The ODMR experiments at 1.6 K were carried out in a 24 GHz spectrometer with the GaN samples placed in the tail section of an optical cryostat. The PL was excited with the 351 nm line from an Ar ion laser with typical power density of ~2 W/cm^2. The ODMR signal corresponds to the change in the PL intensity detected by a Si photodiode that was coherent with the on-off amplitude modulation (~700 Hz–3 kHz) of 50 mW of microwave power while sweeping a dc magnetic field up to 1.1 T. We note that only radiative recombination processes with lifetimes longer than 50–100 ns could yield ODMR signals due to the maximum microwave powers available in these experiments. As required, the PL bands discussed below were separately analyzed with the ODMR technique by placing a combination of visible long-wavelength cutoff and/or bandpass filters in front of the Si photodiode. Finally, for both the EPR and ODMR studies, the GaN samples were rotated in the (1120) planes to obtain defect symmetry information.

For most of the EPR and ODMR reviewed below, the magnetic resonance condition was met for the case of a spin S = 1/2 defect with $h\nu$ (9.5 GHz) = $g\mu_B B_{res}$, where $h\nu$ corresponds to the (fixed) microwave energy, g is the Zeeman energy splitting factor, μ_B is the Bohr magneton, and B_{res} is either the magnetic field position at the zero amplitude crossing of the derivative-like EPR signal or the peak field position of the ODMR absorption-like signal. In addition, the following expression for g-tensors in the case of axial symmetry for a single spin S = 1/2 defect best describes the results of the angular rotation studies: $g(\theta) = (g_{||}{}^2\cos^2\theta + g_{\perp}{}^2\sin^2\theta)^{1/2}$, where $g_{||}$ and $g_{\perp}$ are the g-values with **B** parallel and perpendicular to the c-axis, respectively, and θ is the angle between **B** and the c-axis.

2.2. Samples

The HVPE deposition process of GaN, a fast quasi-bulk growth technique, has been under development for about 4 decades [10]. Presently, GaN wafers between 2 and 6 inches diameter, with thicknesses between 200 to 500 μm, are commercially available. These thick and crack-free GaN films are deposited on various substrates, including sapphire, the sacrificial substrate of choice [11,12]. The substrates are placed on a 1030 °C horizontal susceptor of a hot-wall HVPE reactor. Ga metal and HCl are pre-reacted to form GaCl gas, which is transported by nitrogen carrier gas to the hot growth-zone where it reacts with NH_3 and deposits GaN on (0001) sapphire substrates. For a V/III ratio from 20 to 35, a growth rate between 30 and 100 μm/hr can be reproducibly achieved. These films can be removed from the sapphire substrates by laser-assisted lift-off or by void-assisted self-separation [13,14]. The growth surfaces of such freestanding (FS) GaN templates are extremely rough with large numbers of hillocks, and are inadequate for homoepitaxial growth. Flat, smooth surfaces are obtained after lapping followed by chemical mechanical polishing [15]. These substrates have dislocation densities typically between 10^6 and $10^7/cm^{-2}$, which is orders of magnitude smaller than that of films deposited by MOCVD (metal organic chemical vapor deposition) and MBE (molecular beam epitaxy) methods. In addition, thick films having orders of magnitude lower concentrations of free carriers and semi-insulating (SI) properties can be reproducibly deposited [16].

At present, ammonothermal is the only method to grow large area bulk single crystal GaN boules from a small seed crystal. This method is a modification of the hydrothermal growth technique developed to grow high quality crystalline quartz; whereas water is used as an oxygen source for growing quartz, supercritical ammonia is used as a nitrogen

source for growing GaN [17]. Large ammonothermal GaN (Am-GaN) bulk crystals have been grown with both acidic (e.g., NH_4Cl) and basic (e.g., $NaNH_2$ or KNH_2) mineralizer processes [18,19]. Despite its small crystal growth rate [20] the scalability of the autoclaves, the large number of seeds that can be placed simultaneously, and the ability to sustain growth for many hundreds of hours can overcome the small growth rate disadvantage. Presently, ammonothermal *c*-plane GaN wafers of up to 50 mm in diameter, and smaller dimension *a*-plane and *m*-plane GaN substrates, are commercially available. These wafers are characterized by low dislocation densities (typically $<10^5/cm^{-2}$), very narrow XRD (0002) rocking curves (typically $\leq$20 arcsec), and small curvature radii (between 100 m to 1000 m) [21]. Unfortunately, Am-GaN wafers commonly have a very high concentration of free electrons (typically $>5 \times 10^{18}/cm^3$), which is detrimental to the fabrication of devices that require low free carrier concentration or SI substrates.

Considering the distinct intrinsic properties of GaN crystals grown by these two methods, it seems that a combination of the HVPE technique (higher growth rate and higher purity) and the ammonothermal method (higher structural quality) could introduce a new approach to grow low defect density GaN with controllable electronic properties. Sochacki et al. recently demonstrated that crack-free, high crystalline quality GaN with reduced free carrier concentrations can be deposited homoepitaxially on Ammothermal-GaN (Am-GaN) substrates using the HVPE technique [22]. Also, it has been demonstrated that HVPE-GaN/Am-GaN substrates can be used as seeds for crystal growth or as substrates for epitaxial growth [23]. The present manuscript reviews in detail the intrinsic crystalline, optical and defect properties of heteroepitaxial films, thick free standing HVPE films, and HVPE-GaN films deposited on Am-GaN substrates.

3. Experimental Results and Discussion

3.1. Raman Spectroscopy

Heteroepitaxial growth of GaN on sapphire necessarily results in defects and strain due to the lattice mismatch and sapphire's larger coefficient of thermal expansion [24]. Because the thermal expansion coefficient of GaN is smaller than that of sapphire, the GaN layer becomes compressed and the wafer bends to be convex. Figure 1 shows $z(yy)\bar{z}$ Raman back-scattering measurements made on an HVPE-GaN /sapphire sample's m- and a- plane faces polished for cross-section measurements [25]. The spectra in Figure 1 show that as growth progressed the frequency and FWHM of the E_1(LO) phonon line decreased, consistent with a decrease in free-carrier concentration (the energy position of E_1(LO) mode is very sensitive to excess of free carriers present in the crystal). When comparing c-plane backscattering $z(yy)\bar{z}$ measurements on a later-growth surface to an earlier growth surface, a small downward shift of the $E_2{}^2$ phonon was also observed (the energy position of E_2 mode is very sensitive to stress present in the crystal), consistent with a slight relaxation in biaxial stress with increasing growth. The price paid for the low strain is an increased presence of structural defects.

The lattice mismatch with the sapphire substrate gives rise to the occasional large extended defect such as that seen in Figure 2. Figure 2a shows an 80 μm × 80 μm spatial Raman map of the strain-sensitive $E_2{}^2$ phonon measured on the N-face of an HVPE-GaN growth on sapphire; a clear dipole strain pattern is observed within a 12-sided structure. Figure 2b is a Raman map over the same region of the free-carrier sensitive A_1(LO) phonon; it shows a lower free-carrier concentration within the 12-sided structure. This general behavior was observed for many such defects.

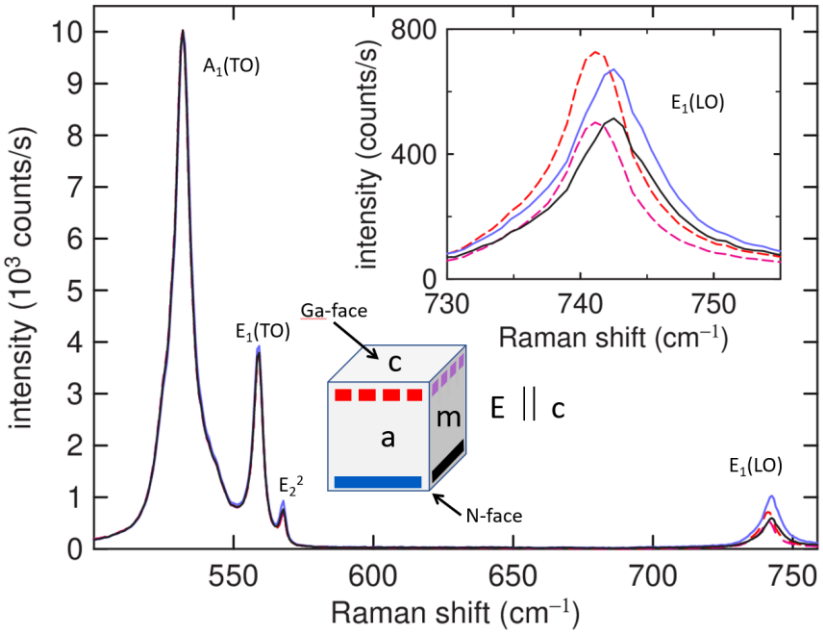

Figure 1. Raman spectra showing reduction of free-carrier concentration with continuing HVPE growth in c direction. Raman spectra measured for both m-plane and a-plane cross-sections of the c-plane growth using photons polarized parallel to the c axis. Measurements on early and later growth ends of both faces are consistent with free-carrier concentration decreasing as growth progresses.

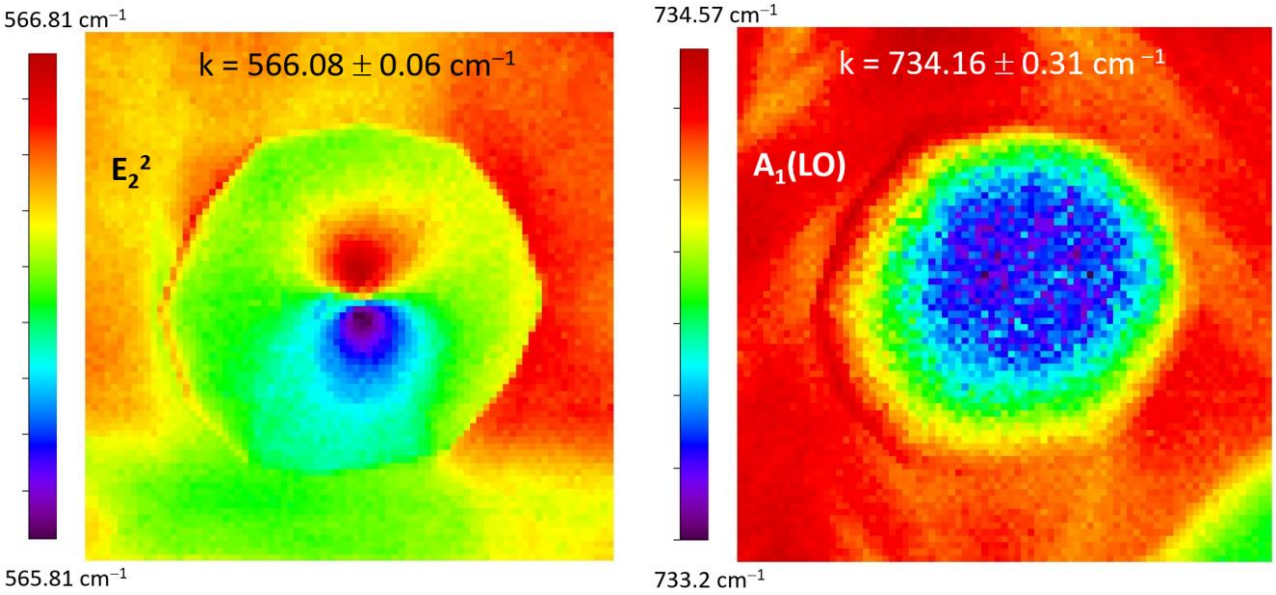

(**a**) (**b**)

Figure 2. Raman spatial map (80 µm × 80 µm) of (**a**) the phonon energies of the strain-sensitive $E_2{}^2$ and (**b**) the free-carrier-sensitive A_1(LO) phonons. Note the strain-dipole pattern in the 12-sided central region, that region having lower free-carrier concentration.

High crystalline quality GaN substrates are needed for the growth of epitaxial GaN films having lower dislocation densities. Figure 3 shows room temperature measurements of the first order RS spectra of m- and c-plane of SI and unintentionally doped Am-GaN samples. Peak positions and reduced line widths of the observed first order phonons indicate good crystalline quality and lower biaxial stress of the Am-GaN wafers. These observations are consistent with results published by Gogova et al. Ref. [26] for m-plane

non-intentionally doped substrates. A high background concentration of free-electrons, caused by a high concentration of uncompensated shallow donors, results in the formation of a free-carrier collective mode (plasmon) with low and high dispersion curves, ω^- and ω^+, seen in Figure 3b. The plasmon modes couple with the polar phonons [A_1(LO) and E_1(LO)] introducing the new vibrational mode LPP (LO-phonon-plasmon coupled mode); whose peak positions increase with increasing free-electron concentration. Spectral analysis of the LPP can be conveniently used to estimate the residual doping level of the samples [27,28].

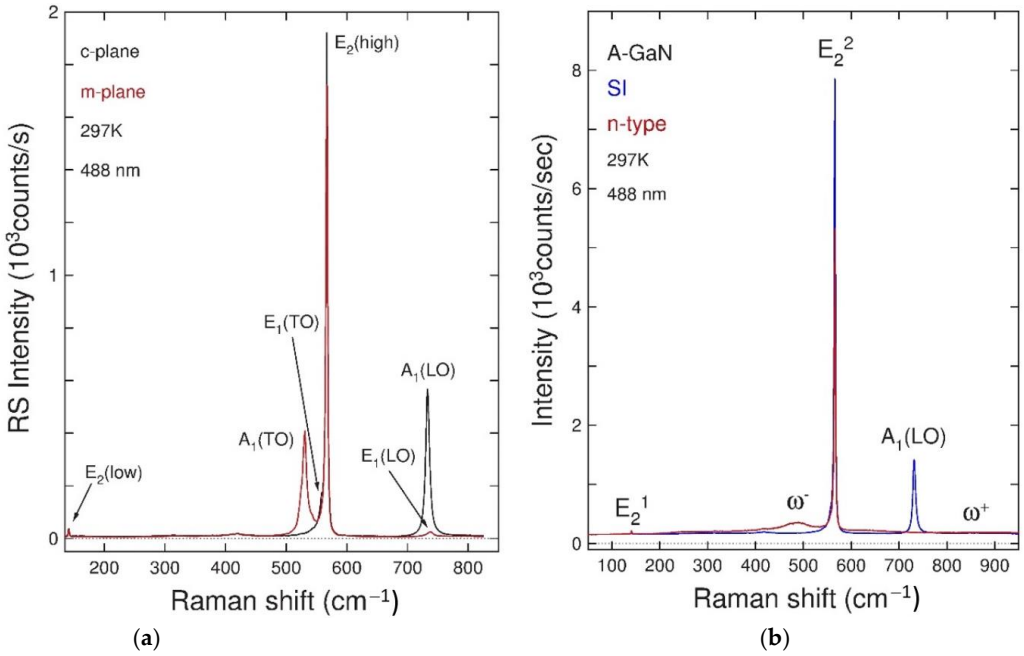

Figure 3. (**a**) First order Raman spectra of c- and m-plane SI ammonothermal GaN. (**b**) First-order Raman spectra of SI and n+ c-plane Am-GaN samples. The latter highlights the ω^- and ω^+ plasmon modes, LPP^- and LPP^+, respectively [29].

The spectra of SI wafers highlighted in Figure 3a, which do not have the LPP modes, indicate that wafers with low effective free-carrier concentration may be obtained by doping with compensating acceptor impurities during the growth. A high background concentration of shallow donors requires a higher concentration of compensating acceptors; this affects the crystalline quality and other intrinsic properties of the substrates and limits potential applications. The ammonothermal growth processes must be improved to reduce the pervasive high residual concentration of oxygen. Recently this high concentration of oxygen was reduced by the use of getter in ammonothermal growth [30].

Raman mapping measurements of HVPE GaN grown on high crystalline quality Am-GaN reveal that the strain-sensitive E_2^2 phonon's frequency shows negligible strain across the growth surface, and that the strain remains negligible as growth proceeds [31]. Measurements of the free-carrier sensitive A_1(LO) phonon revealed a free carrier concentration low compared to that of the Am-GaN substrate. The free-carrier concentration was observed to increase as HVPE growth proceeded, thus motivating SIMS measurements. SIMS measurements revealed increasing levels of Si with growth, likely due to Si being etched from the quartz elements of the growth reactor.

While Am-GaN generally has a higher crystalline quality, some large-scale defects are observed in HVPE-GaN grown on it. The nature of such defects can be probed using Raman scattering measurements. Figure 4 shows 128 μm ×112 μm spatial maps of the Raman shift of the free-carrier sensitive A_1(LO) line and the strain sensitive E_2^2 line. While the strain (Figure 4b) is localized around the visible defects (Figure 4a), the free-carrier

concentration (Figure 4c) is affected over a wider region and hints at the presence of a defect not clearly seen in the optical image.

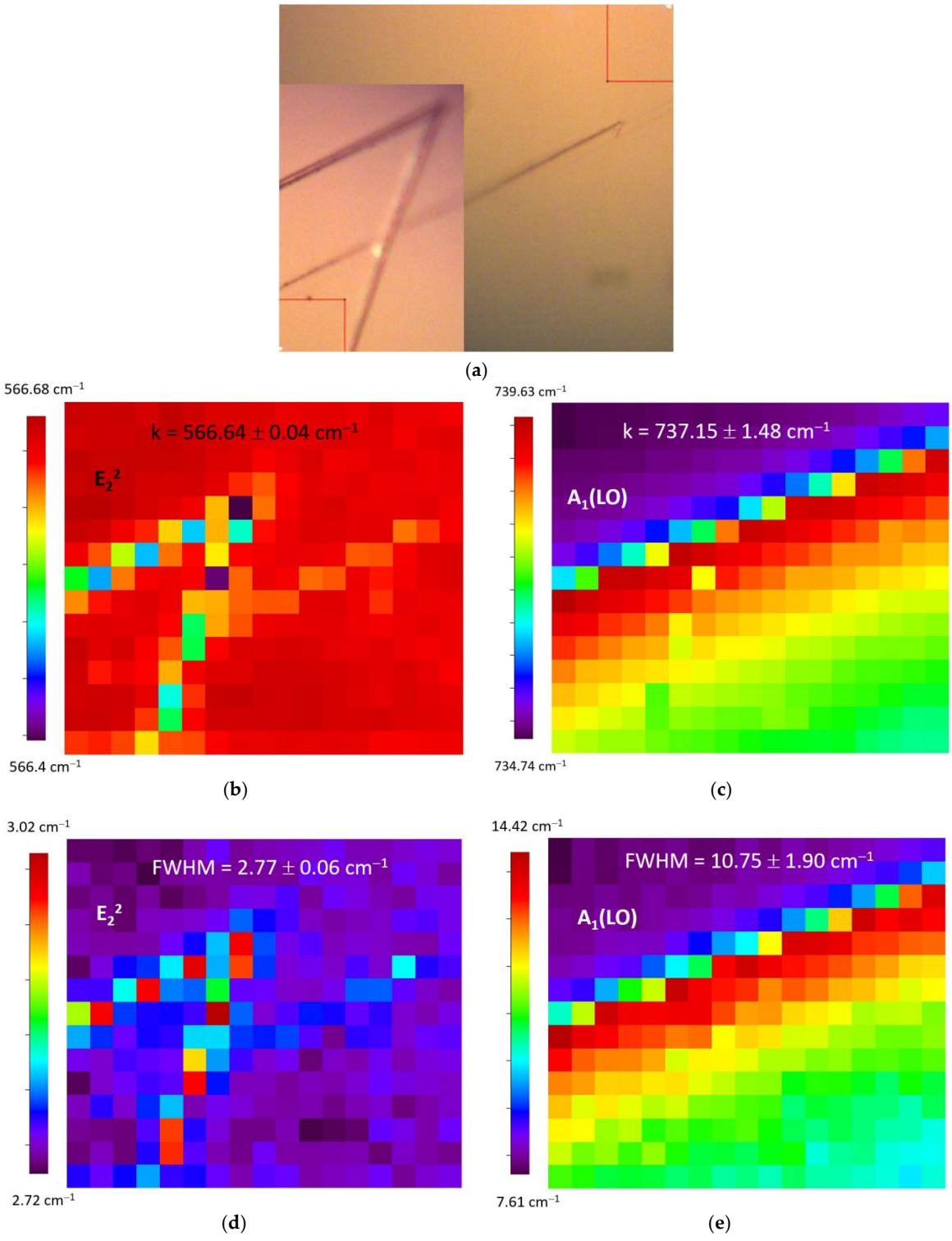

Figure 4. (**a**) Optical image of extended defects in a 128 µm × 112 µm region on the Ga-face of an HVPE-GaN film grown on Am-GaN. Raman map of the frequency of the (**b**) strain-sensitive E_2^2 phonon and the (**c**) free-carrier sensitive A_1(LO) phonon over the region shown in (**a**). (**d**,**e**) are maps of the FWHM of these Raman lines.

3.2. PL

The low temperature PL spectra, covering a wide spectral range (1.75–3.55 eV), of unintentionally doped (UID) GaN heteroepitaxial films usually are dominated by a relatively sharp emission band around 3.47 eV (near band edge [NBE] emission), with full-width-half-maximum (FWHM) typically $\leq$3.0 meV and a broad featureless band peaking near 2.25 eV, the so called yellow band (YB) [32]. The former is assigned to recombination processes involving the annihilation of excitons bound to neutral donors (BE) and a weaker free-excitons (FE) emission band, and the latter to a complex defect involving impurities and native defects [32,33]. Low-resolution/wide-energy range spectra of a UID freestanding HVPE GaN wafer, also characterized by an intense NBE emission band, are highlighted in Figure 5 [34]. A broad YB emission band is also observed but overlapped with a weaker green emission band. Also observed is a relatively weaker emission band associated with processes involving the recombination of electrons bound to shallow donors with holes bound to shallow acceptors. This emission band, commonly called donor-acceptor pair (DAP) band, is characterized by the presence of a non-phonon line at 3.27 eV (non-phonon/zero phonon line, ZPL), which does not involve a longitudinal optical (LO) phonon in the recombination process, and its phonon replicas, displaced by 92 meV, the LO phonon energy [34,35]. The shallow acceptor associated with this DAP emission band is magnesium ions, an impurity trace present in the precursors, the acceptor of choice for p-type doping [35]. The observation of a sharper BE emission band (FWHM = ~1.0 eV) and its phonon replicas, and relatively intense and sharper light- and heavy-holes related FE emission lines, in the higher resolution spectra, is a clear indication of improved crystalline and electronic properties [34] of the HVPE sample.

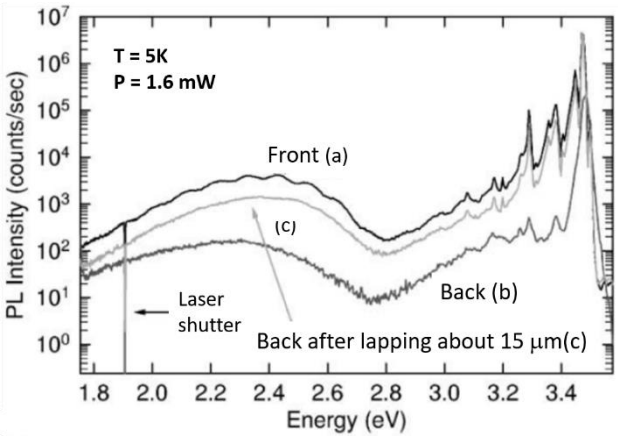

Figure 5. Low resolution 5 K PL spectra, acquired between Near-UV-to-Near-IR spectral region, of a FS HVPE GaN sample. Note the spectral variations between the spectrum acquired at the growth face (Ga-polar face) and the substrate- interface surface (N-polar face) [34].

The high spectral resolution (band pass < 100 μeV) PL measurements carried out at 5 K under several laser excitation densities, in the excitonic spectral region, of a freestanding HVPE-GaN sample with carrier concentration ~2 $\times$ 10^{16} e/cm^3 and dislocation density $\leq$ 10^7 cm^{-2}, are depicted in Figure 6. The dominant spectral feature in all spectra is the emission band associated with the recombination process that leaves the donor in the ground state after the exciton annihilation, often designated I^O_2, with center around 3.4714 eV. This emission band is composed of three peaks at 3.4714, 3.4718, and 3.4722 eV, which have been assigned to excitons bound to neutral oxygen donors ($O^0_N X_A$) on the nitrogen sites, neutral unidentified donors ($D^0_? X_A$), and neutral Si donors on the G_a sites ($Si^0_{Ga} X_A$), respectively [36]. These assignments were determined by comparing the present results with detailed high-spectral resolution FTIR and high-sensitivity SIMS studies [37] of this sample. Weaker, but observable, are emission bands assigned to recombination involving the FE associated with holes from valence band A around 3.4784 eV, the free

exciton involving holes from valence band B at 3.4843 eV, the exciton B bound to the O donors on N site at 3.4753 eV, the exciton B bound to Si donors on the Ga site at 3.4758 eV, and the A-valence band exciton bound to neutral Mg acceptors at 3.466 eV [38]. Figure 7. shows luminescence spectra of the commonly called "Two-electron satellite" (2ES) region, acquired with temperatures between 5 and 25 K, associated with recombination processes that leave the O and Si donors at the excited states after exciton annihilation. All major emission features observed in this spectrum have been assigned, and they are consistent with the donor excitation spectra obtained from infrared transmission [39], which confirm the ground state binding energies for Si_{Ga} and O_N are 30.18 and 33.20 meV, respectively. The observation of a NBE spectra with many sharp emission lines verify improved crystalline quality of these GaN wafers deposited by the HVPE method.

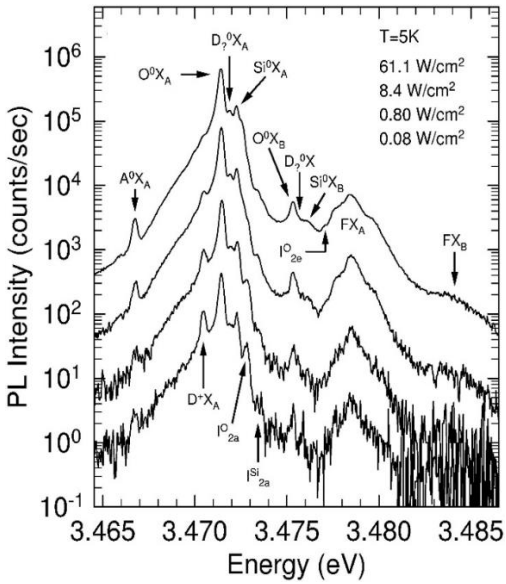

Figure 6. High-resolution and low temperature PL spectra of a FS HVPE sample, with low carrier concentration (~2 × 10^{16} e/cm^3), acquired at the exciton ground state spectral region with different laser power densities. The line assignments are discussed in the text [36].

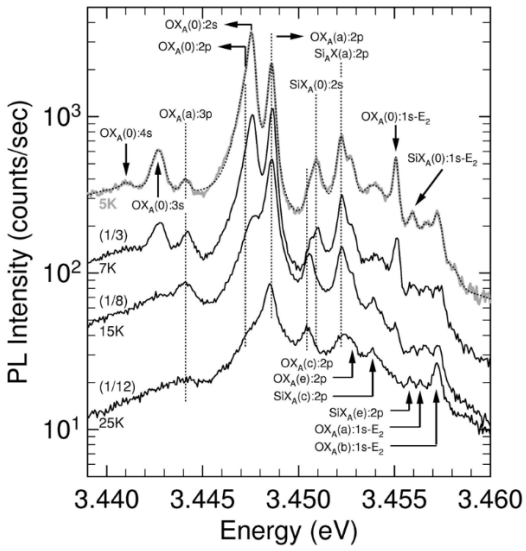

Figure 7. High-resolution PL spectra of the FS HVPE sample depicted in Figure 6, acquired at 4 temperatures, at the spectral region commonly called "Two-electron satellite" (2ES). The line assignments are discussed in the text [36].

Because of the excess of shallow oxygen donors in Am-GaN, achieving semi-insulating material requires doping with acceptors (e.g., zinc and magnesium). Low temperature photoluminescence spectra of unintentionally doped (UID) a- and m-plane Am-GaN wafers, and an Mg-doped c-plane Am-GaN wafer are depicted in Figure 8. The spectrum of the m-plane sample (purple line) shows a dominant sharp NBE emission band; a clear fingerprint showing the presence of shallow Mg-acceptors is the weaker DAP band at 3.27 eV (with phonon replica 92 meV lower). This spectrum also shows a more intense broad emission band with peak near 2.9 eV previously assigned to Zn-acceptors [40]. It is believed that the observation of weaker DAP bands is related to reactor memory from previous Mg doping growth runs. The spectrum of the a-plane sample (red line) exhibits much weaker PL than that observed for the m-plane sample, a broader and high energy shifted NBE, a Zn-related DAP band and a negligible contribution from the Mg-related DAP emission band. SIMS analysis of bulk Am-GaN indicates that H and O are the main unintentional impurities. Mg, Zn, and Mn (2.6 eV) acceptors are also incorporated at much lower levels, consistent with the observation of these DAP related emission bands [41]. The spectra of the c- (Ga-face) and -c-plane (N-face) are represented by the blue and green lines, respectively. Dominant Mg related DAP emission bands are observed from both faces, however that measured at the N-face is 6 times more intense than that measured at the Ga-face, while the NBE intensity is substantially reduced. Similar observation was verified from GaN platelets grown by Na-based solution growth, also a thermo-equilibrium growth method, suggesting that higher incorporation of Mg occurs at the N-face [42]. Note that the intensity of the DAP emission band is much larger than the NBE emission intensity in the c-plane sample spectra, while the opposite ratio is observed in the spectra for the m- and a-plane samples. This suggests that the high concentration of unintentional acceptor impurities doping may result from reactor memory effects after the growth of Zn- and Mg-doped samples.

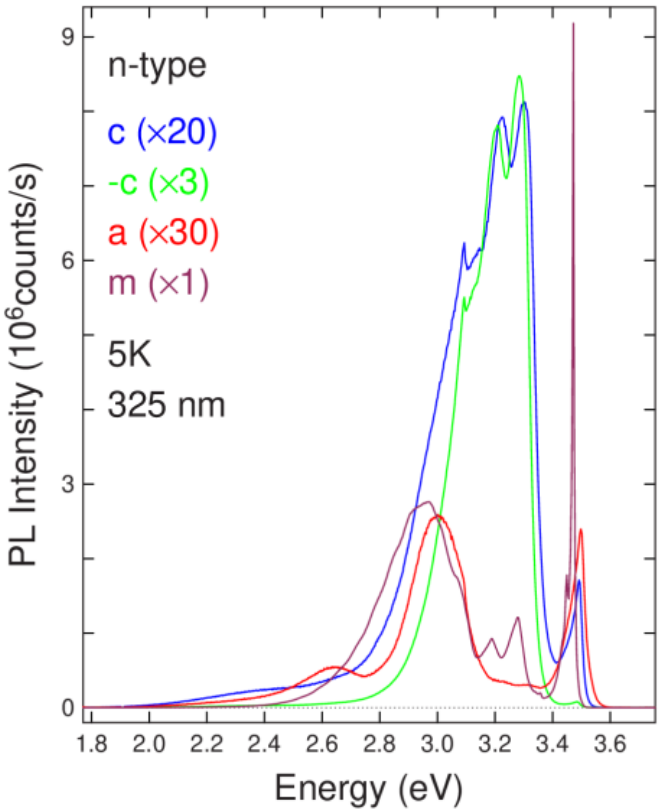

Figure 8. Low temperature photoluminescence spectra of Mg doped c-plane GaN, and UID a- and m-plane Am-GaN. Low intensity DAP emission bands observed in the spectra of the a- and m-plane wafers are consistent with reactor doping memory [29].

Figure 9 shows the low temperature photoluminescence spectra of nominally semi-insulating a-, c-, and m-plane Am-GaN wafers. These samples were grown by introducing an oxygen getter, to reduce the concentration of oxygen from 2×10^{19} cm^{-3} to 1–2 $\times$ 10^{18} cm^{-3}, and compensating the remnant by adding 1–2 $\times$ 10^{18} cm^{-3} Mg acceptors. Note the absence of any NBE emission in all three spectra, indicating that the shallow donors have been fully compensated by the incorporation of Mg acceptors.

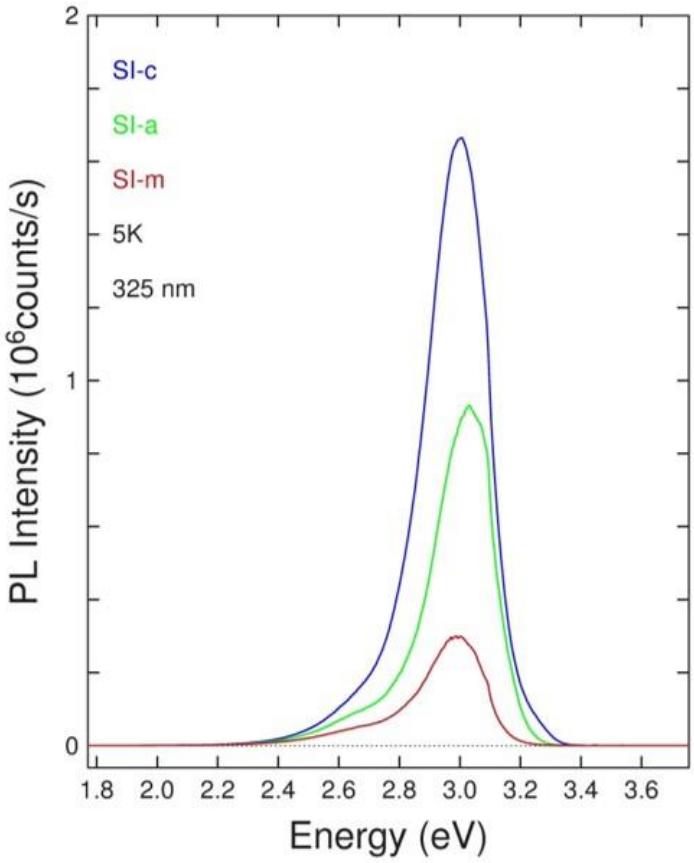

Figure 9. Low temperature photoluminescence spectra of SI a-, c-, and m-plane wafers. Note the absence of any NBE emission bands [29].

As previously mentioned, the knowledge of the intrinsic properties of GaN, and the identification of the pervasive impurities and intrinsic point defects can be conveniently used to detect and identify their incorporation and activation during bulk growth and film deposition. In fact, we have recently used this knowledge to investigate the incorporation of Si and O in thick FS GaN films deposited by HVPE on HVPE-GaN/ammonothermal-GaN templates. These thick freestanding films have close to perfect crystallinity, with more than two orders of magnitude reduced free carrier concentration relative to the Am-GaN substrate [24]. These thick films show uniform optical and electronic properties across the interface and growth surface regions, as measured by Raman scattering, PL, and SIMS, but show a 10 fold increase of Si impurity concentration as the growth proceeds [31]. Despite that, the room temperature mobility is over 800 cm^2/Vsec, and the FWHM linewidths of the bound exciton lines at 3.4716 eV ($O^0X_A{}^1$) and 3.4724 eV ($Si^0X_A{}^1$) are only 146.4 μeV and 185.0 μeV, respectively (see Figure 10). These smaller FWHM linewidths were acquired for the N-polar face of the sample, which has 2.0 $\times$ 10^{16} Si/cm^{-3} (10 times less than the Ga-polar face), indicating that increasing shallow impurity concentration introduces spectral line broadenings of both the donor FTIR excitation spectra and the exciton PL spectra [43]. These considerably smaller FWHM linewidths observed in the N-polar face of a homoepitaxial HVPE GaN sample (more than 50%) in comparison to that

observed in the Ga-polar face of a freestanding/heteroepitaxial HVPE GaN sample having similar concentrations of O and Si, indicates a considerable reduction of the inhomogeneous broadening, typical for heteroepitaxial FS HVPE GaN film spectra [44]. This observation confirms improved crystallinity quality of homoepitaxial samples. Recently, Fujikura and co-workers proposed a new approach to reduce the undesirable incorporation of pervasive shallow donors in HVPE GaN films, which will allow the realization of new kinds of electronic devices [45].

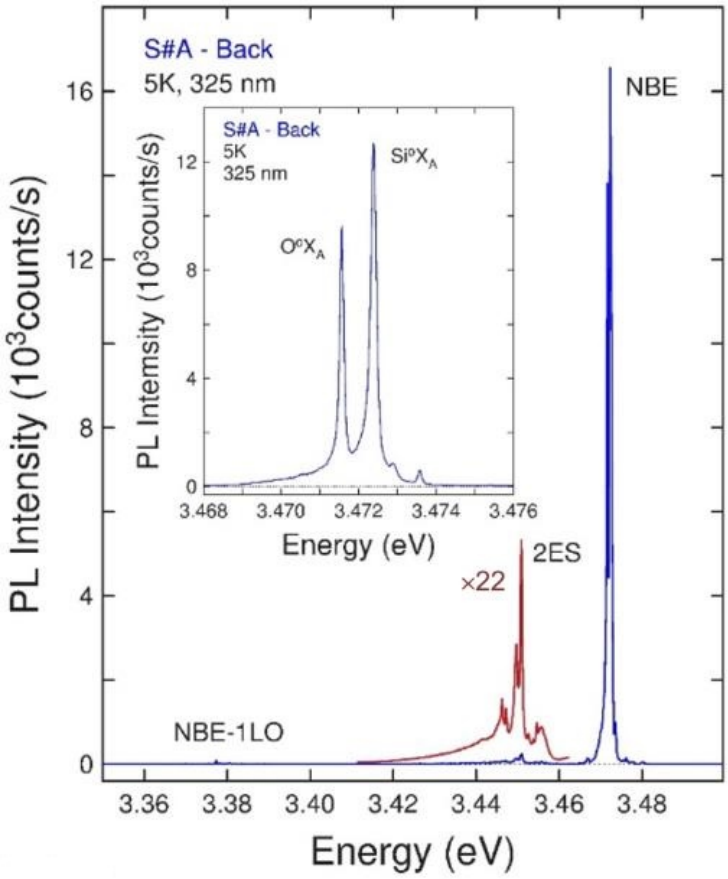

Figure 10. Low temperature, high-resolution PL spectra of the N-polar face of a FS HVPE GaN sample deposited on HVPE-GaN/Am-GaN template. The insert attests the sharpness of the bound exciton emission lines, and confirms the high crystalline quality of this sample [43].

The excess of free carries in unintentionally doped (UID) HVPE GaN results mostly from the undesirable incorporation of shallow Si and O donor impurities during the films deposition. These films are inadequate for high-power/high-frequency and high-voltage vertical devices, which require semi-insulating (SI) substrates and thick blocking layers with $\leq 1 \times 10^{15}$ electrons/cm^3, respectively [46]. SI GaN substrates have been produced by adding C or Fe precursors during growth, which introduce deep compensating levels in the GaN bandgap [47,48]. High concentrations of shallow donors require higher concentrations of compensating impurities, which may degrade the intrinsic material properties [49,50]. C impurities have been associated with two gap levels in GaN; namely the well know yellow emission band at 2.25 eV and the so-called "blue-band" ~3.0 eV. Fe seems to be the most adequate impurity because the $Fe^{3+/2+}$ acceptor level is about 0.34 eV below the bottom of the conduction band [47]. Therefore, it is expected that this deep acceptor level will efficiently compensate the GaN free carrier at the typical devices operating temperatures. However, organic-metallic Fe precursors such as cyclopentadienyl iron results on unintentional C co-doped films [51]. To avoid C incorporation, a new iron precursor was developed [52]. Low temperature PL measurements verified that the intensity of the NBE emission, associated

with recombination processes involving shallow Si and O donors, reduces by several orders of magnitude with increasing concentration of Fe impurity, consistent with increasing compensation of these shallow donors. Fe incorporation and activativation was confirmed by the near-IR low temperature PL measurements, as depicted in Figure 11. In this figure, we clearly observed the peak assigned to the $^4T_1(G)$–$^6A_1(S)$ crystal-field transition (the zero phonon line (ZPL) at 1.299 eV). All emission lines present in this spectrum have been previously detected and identified [53].

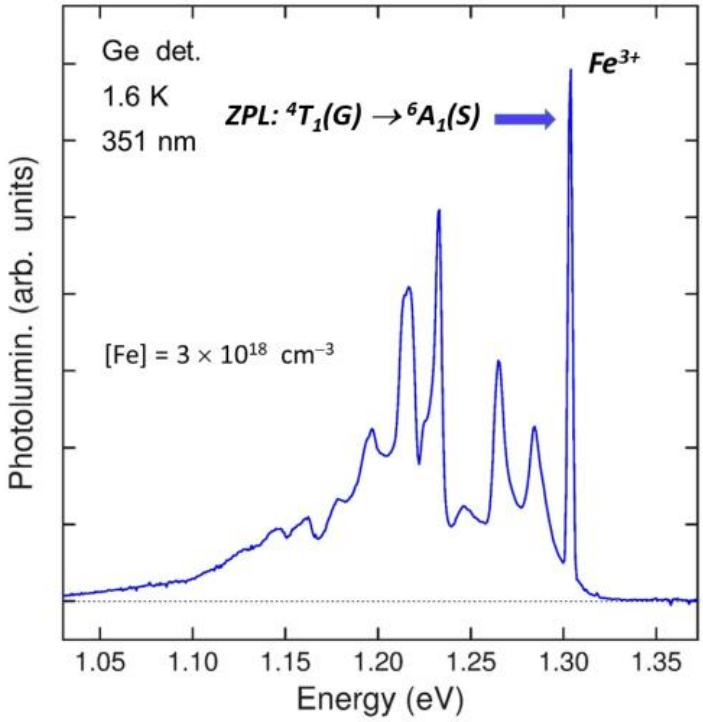

Figure 11. Infrared PL spectrum of a Fe-doped HVPE GaN sample excited with the 351 nm laser line of Ar-ion laser, acquired at 1.6 K [52].

3.3. Magnetic Resonance

3.3.1. EPR

EPR is valuable measurement technique for obtaining information on the concentration and (n- or p-) conductivity type of free carriers in GaN thin films and bulk substrates. A representative classic example is provided in Figure 12 for three GaN bulk samples (1 mm thick) grown by HVPE with the applied magnetic field, **B**, oriented parallel to the c-axis [54]. The samples were unintentionally doped but detailed SIMS analyses revealed oxygen and silicon shallow donor impurities and, in some cases, compensating carbon impurities above their respective detection limits. We note that O is the residual impurity with the highest concentration in these three samples. Though other compensating acceptor-like centers may be present, we label each of the spectra by the net concentration of shallow donor centers (i.e., [O] + [Si] − [C]) as provided by the SIMS measurements. A single EPR line at 15 K with axial symmetry was observed for each sample with $g_{||} \sim g_{\perp} \sim 1.95$ and with varying FWHM linewidths (6–18 G). Most notably, this resonance was firmly established by several groups [55–57] as a "fingerprint" of shallow donors/conduction electrons in GaN and its observation gives definitive proof of the n-type character of these samples. Unfortunately, due to the absence of resolved electron-nuclear hyperfine structure it is not possible to assign this EPR feature with Si or O impurities that are well-known sources of n-type conductivity in GaN. A clear trend found for these spectra is the decreasing FWHM linewidth for samples with increasing (uncompensated) shallow donor concentration. This 'motional narrowing' behavior can be understood as the averaging out of the electron-

nuclear hyperfine interaction between the donor electron spin and the nuclei of the host lattice atoms as discussed in previous EPR studies of n-type GaN [55].

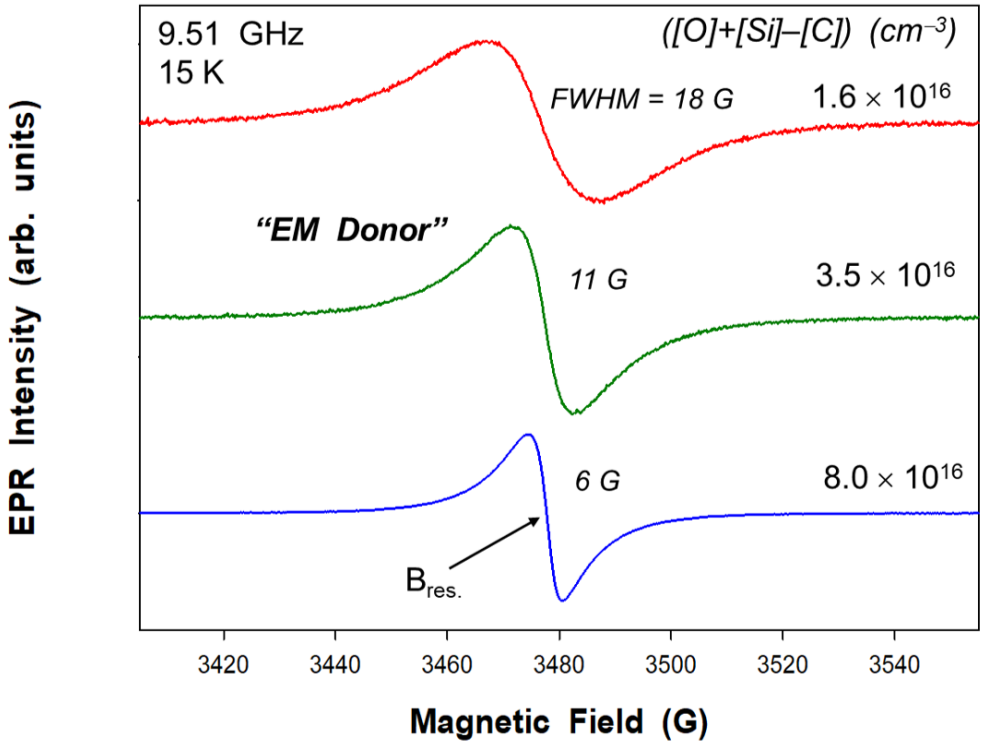

Figure 12. EPR spectra obtained at 15 K with **B** | | c-axis for three HVPE-grown (unintentionally doped) n-type GaN bulk samples. B_{res} corresponds to the zero-amplitude crossing of these derivative-like EPR signals.

As discussed above, the intentional introduction of Fe impurities during growth is often employed to produce semi-insulating bulk GaN. Especially for thick GaN substrates grown by HVPE, such deep level acceptor centers with concentrations of ~10^{16}–10^{18} cm^{-3} are very effective in compensating residual Si and/or O shallow donors and, thus, make such Fe-doped GaN substrates very useful as templates for high power/high temperature device applications. Similar to the example given above for shallow donors, EPR provides a characteristic signature for the incorporation and activation of Fe centers on the host Ga lattice sites in GaN. As an example, EPR spectra at 300 K for nominal undoped and intentional Fe-doped HVPE-grown GaN substrates (1 mm thick) are shown in Figure 13 [52]. These samples were also well characterized by SIMS to obtain the background C, O, and Si impurity concentrations and the Fe doping levels. The sample "3C" with an Fe doping concentration of 3 × 10^{18} cm^{-3} exhibited a 5-line EPR pattern (green vertical arrows) with the magnetic field applied parallel to the c-axis that has been firmly associated with spin S = 5/2 Fe^{3+} ions substitutional on the Ga lattice sites (2S = 5 EPR lines) [58,59]. In contrast to the case for shallow donors in GaN, we note that the long spin-lattice relaxation times associated with the Fe^{3+} ions make it possible to observe strong EPR signals at room temperature. This situation is shown in Figure 13, where no EPR signals above the noise level were found at room temperature for the reference GaN substrate sample. SIMS on this GaN substrate revealed a residual Fe concentration of 3 × 10^{15} cm^{-3}, due to so-called 'memory' doping, that was lower than the residual Si impurity concentration. As a result, all of the Fe in this sample was compensated by the Si impurities such that the Fe ions were in the 2+ non-paramagnetic charge state.

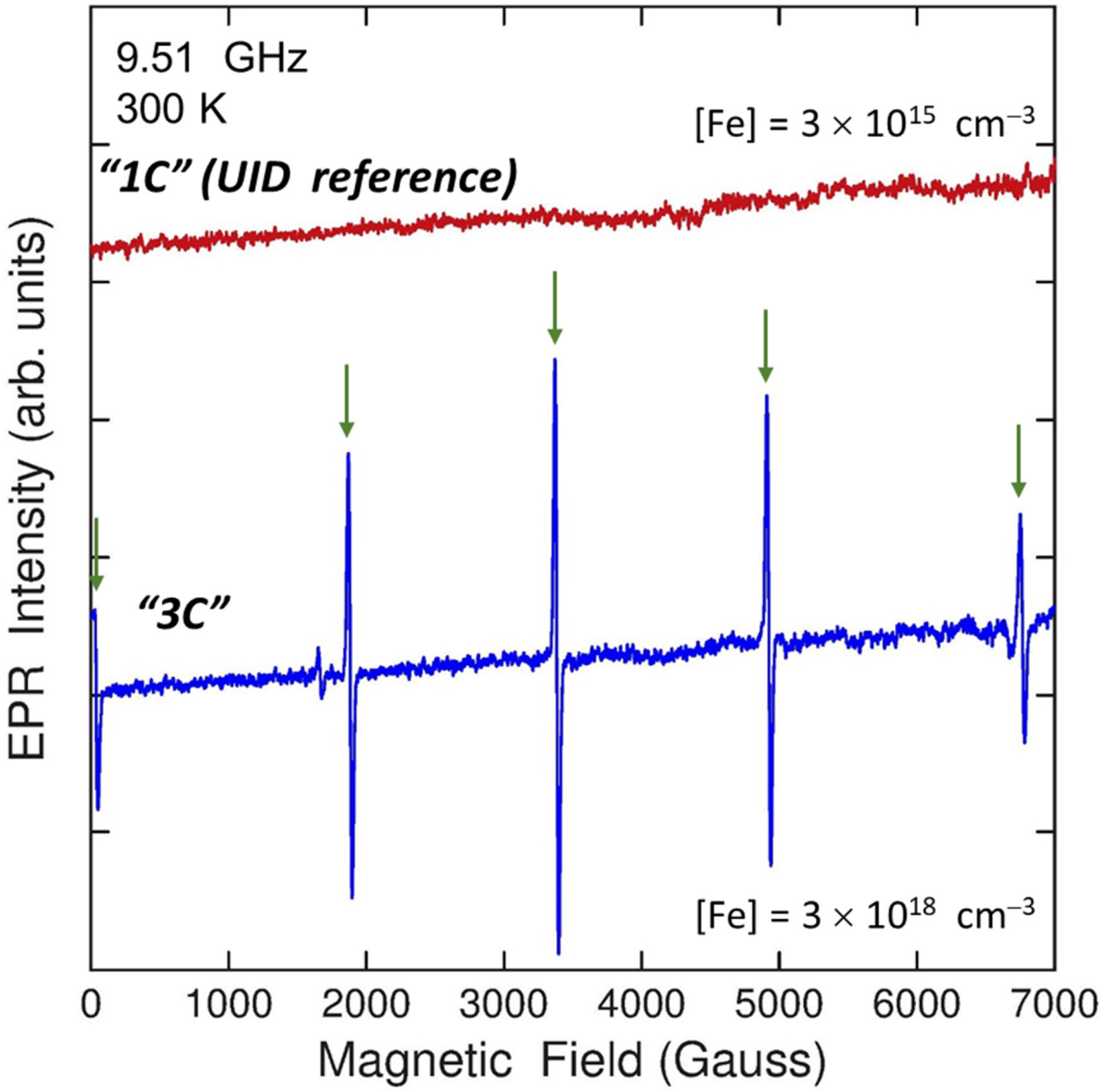

Figure 13. EPR spectra found at 300 K for unintentional and Fe-doped HVPE-grown GaN bulk samples with **B** oriented along the c-axes. The five-line spectrum (vertical green arrows) is associated with substitutional Fe^{3+} ions on the Ga lattice sites.

3.3.2. ODMR

Due to its technological importance for p-type doping in GaN, Mg impurities have been the subject of numerous optical and magnetic resonance investigations. The power of the ODMR technique has been very well demonstrated from a variety of studies on Mg-doped GaN hetero- and homoepitaxial layers and bulk substrates. A clear example of this is shown by the strong ODMR signals obtained on the 3.27 eV shallow donor–shallow acceptor (SD-SA) emission band observed from an HVPE-grown GaN bulk substrate (1.1 mm thick) with a Mg doping level of 4×10^{17} cm^{-3} [60]. The PL found at 2 K between 1.8 and 3.5 eV from this sample is shown in Figure 14 and is very similar to that reported in Ref. [61] for a "sister" GaN substrate sample with Mg doping concentration of 3×10^{18} cm^{-3}. The PL is dominated by an intense emission band at 3.467 eV due to the annihilation of excitons bound to the shallow neutral Mg acceptor impurities. In addition, this sample exhibits an emission band at 3.27 eV and a series of LO phonon replicas at lower energies. The shift of the 3.27 eV band (and phonon replicas) by 5 meV to lower

energies with a 1000-fold reduction of the excitation power density supports an assignment of this emission to recombination between residual shallow donors (either Si and/or O impurities as revealed in SIMS measurements) and shallow Mg acceptors.

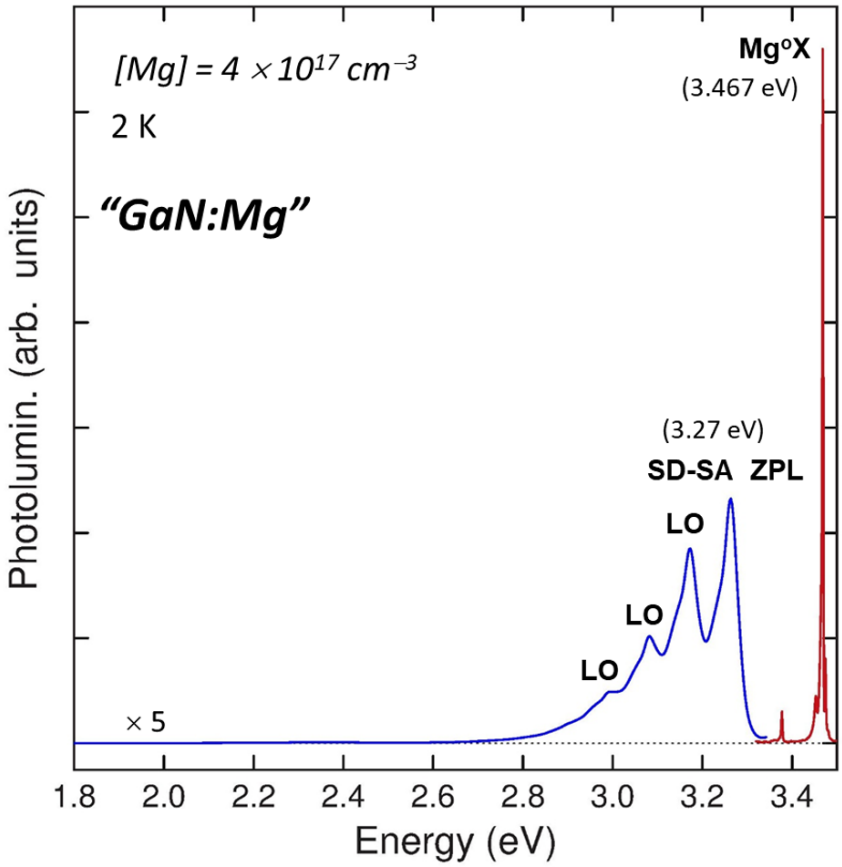

Figure 14. PL at 2 K between 1.8 and 3.5 eV from an HVPE-grown GaN bulk substrate doped with 4×10^{17} cm^{-3} Mg impurities.

Figure 15 shows ODMR at 24 GHz obtained using the 3.27 eV SD-SA PL band of a bulk GaN sample having [Mg] = 4×10^{17} cm^{-3} for several orientations of the applied magnetic field with respect to the c-axis. Two luminescence-increasing signals are found that further support the assignment of this emission to SD-SA recombination. The first (labeled SD) is sharp (FWHM ~ 7–8 mT) and is slightly anisotropic (as indicated by the dashed vertical line) with $g_{||} = 1.952$ and $g_{\perp} = 1.949$. These g-values are the same as found from EPR studies of n-type GaN as described above and, thus, assigned to shallow donors (either residual O and/or Si impurities as revealed in the SIMS measurements). The second feature (labeled Mg) is broader (FWHM ~16–20 mT for angles $\leq 25°$), exhibits weaker intensity for **B** within 10° of the c-axis, and shifts rapidly to higher field (as denoted by the purple vertical arrows) with **B** rotated away from the c-axis. We note the same resonance was reported from EPR of this sample [61]. Figure 16 shows a plot of the g-values (green crosses) of this ODMR signal and those (green circles) from EPR measurements of this same sample as a function of the angle (θ) between **B** and the c-axis. An excellent fit to this data using the usual expression for g-tensors in the case of axial symmetry (given in the Technical Approach section) is obtained with $g_{||} = 2.19 \pm 0.01$ and $g_{\perp} \sim 0$. Most notably, such a highly anisotropic g-tensor is predicted from effective mass theory [62] for shallow acceptors in wz-GaN where the ground state (from symmetry arguments) reflects the character of the (heavy hole) $J = 3/2$, $m_J = \pm 3/2$ valence band edge. Thus, the resonance is ascribed to the Mg shallow acceptor centers. We note this same ODMR feature (blue triangles in Figure 16) was also observed on the 3.27 eV SD-SA PL from a 1.5 μm-thick, MBE-grown GaN homoepitaxial

layer doped with [Mg] = 1×10^{17} cm^{-3} [63]. This behavior contrasted significantly with all previous EPR and ODMR investigations of Mg-doped GaN heteroepitaxial layers where a signal with a much smaller g-value anisotropy was found. This is shown explicitly, for example, by the g-values (red squares) observed by ODMR on the 3.27 eV SD-SA emission band from a 1.5 μm-thick, MOCVD-grown GaN heteroepitaxial layer with Mg doping level of 2×10^{18} cm^{-3} [64]. The main reason proposed [63] for the observation of the highly anisotropic Mg shallow acceptor magnetic resonance signal is the much reduced dislocation densities ($\leq 10^7$ cm^{-2}) present in the Mg-doped GaN homoepitaxial and thick free-standing bulk substrates relative to those typically found (10^8–10^{10} cm^{-2}) in GaN:Mg heteroepitaxial layers grown by MOCVD and MBE. The random strain fields associated with such high dislocation densities likely produce a symmetry-lowering local distortion of the Mg shallow acceptors [62]. As a result, their ground state wave function is not solely derived from the heavy-hole valence band edge but is a mixture of light ($m_J = \pm 1/2$) and heavy hole ($m_J = \pm 3/2$) valence band character that accounts for the nearly isotropic g-tensors observed for such Mg-doped GaN heteroepitaxial layers in both EPR and ODMR experiments.

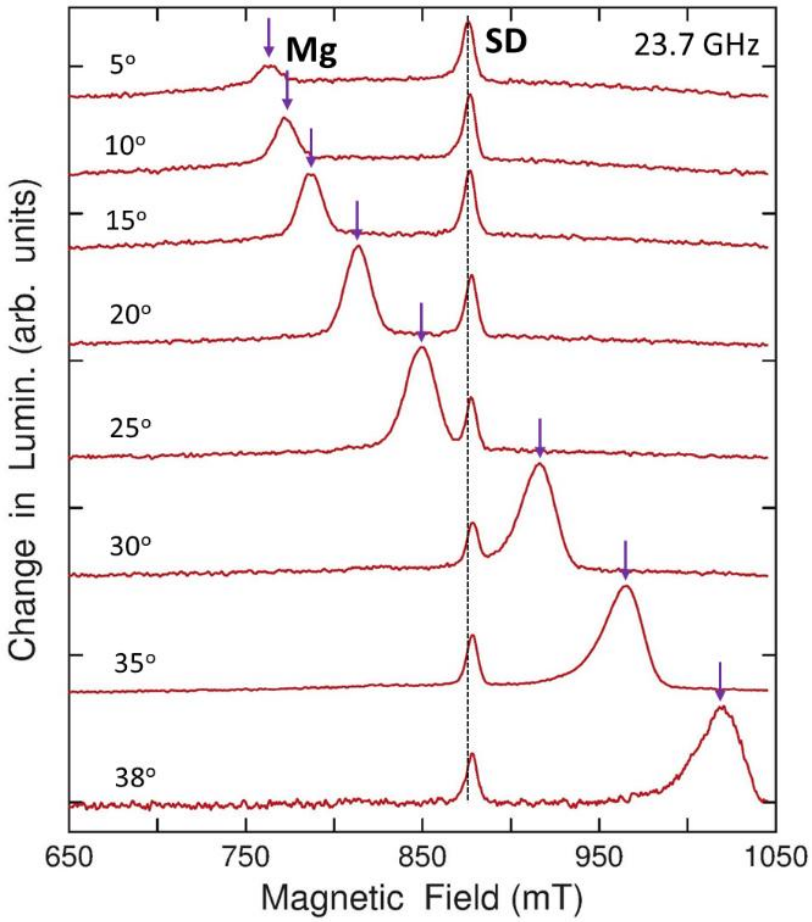

Figure 15. ODMR spectra obtained at 24 GHz on the SD-SA PL from a GaN bulk substrate sample with Mg doping of 4×10^{17} cm^{-3} for several orientations of **B** with respect to the c-axis. The dashed vertical line indicates the small shift found for the shallow donor (SD) signal. Vertical arrows track the strong angular dependence observed for the feature "Mg" ascribed to shallow Mg acceptor centers as described in the text.

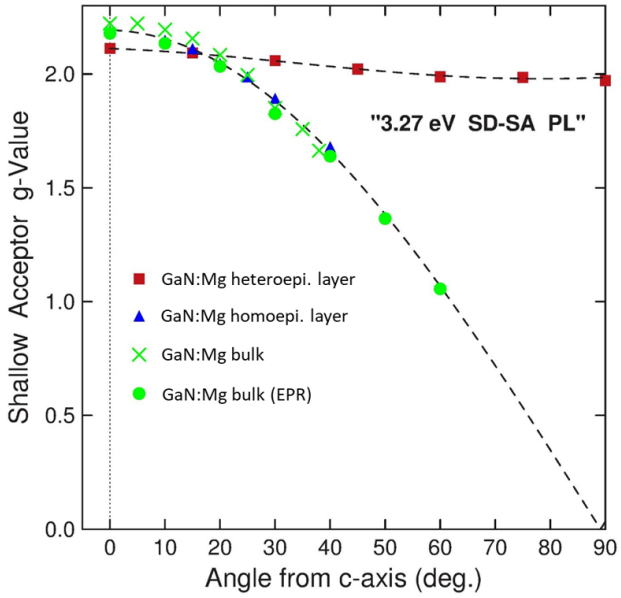

Figure 16. The angular variation of the g-values for ODMR feature "Mg" found on the 3.27 eV PL band from the Mg-doped GaN bulk sample (green crosses) highlighted in this review and those published previously on similar emission from Mg-doped GaN heteroepitaxial (red squares) [64] and GaN:Mg homoepitaxial (blue triangles) [63] layers. The g-values for the strong EPR signal reported for the same Mg-doped GaN bulk substrate sample (green circles) [61] are also shown in this plot. Dashed curves are fits to the data as described in the text.

The electrical and optical properties of carbon dopants in GaN have also been topics of many experimental and theoretical studies over the last 30 years. In particular, carbon has been widely proposed as one of the sources responsible for the so-called broad "yellow" emission band with peak energy near 2.2 eV observed from unintentionally-doped n-type GaN grown by a variety of techniques (including MBE, MOCVD, and HVPE). For this review, it serves again as another demonstration of the power of the ODMR technique to shed light on the nature of these C impurities in GaN. For example, the ODMR at 24 GHz that was separately obtained on the 2.23 eV "yellow" (top spectrum) and 2.95 eV "blue" (bottom) PL bands from a 600 μm-thick, HVPE-grown GaN bulk substrate with carbon doping level of 1×10^{18} cm^{-3} is shown in Figure 17 [65]. These emission bands are displayed in the inset of Figure 17; note that the bandedge excitonic emission was quenched for this level of carbon doping. Two luminescence-increasing resonances are found on each of these PL bands with **B** $\perp$ to the c-axis. The first (labeled SD) is common to each spectrum and is assigned to residual shallow donors (either O and/or Si impurities as revealed in the SIMS measurements) based on its characteristic g-value of 1.95 as discussed above. The second ODMR signal observed on the 2.23 eV PL band has a $g_{\perp}$-value of 1.995 and a FWHM linewidth of ~16 mT. These parameters are very similar to those reported previously by several groups [66–69] for a deep acceptor center typically revealed by ODMR on similar emission from unintentionally doped (n-type) and highly-resistive GaN epitaxial layers. Based on the strong correlation of this emission with C doping and theoretical modeling [r], this feature is ascribed to the (0/-) deep acceptor transition level (located ~0.9 eV above the valence band edge) of the C_N defect center. The second ODMR signal found on the 2.95 eV PL band exhibits slightly different magnetic resonance parameters (as indicated by the dashed vertical lines in Figure 17) with a $g_{\perp}$-value of 2.010 and a FWHM linewidth of ~20 mT. This resonance is tentatively ascribed to the (+/0) deep donor transition level (located ~0.3–0.4 eV above the valence band edge) associated with the C_N defect centers as modeled in Refs. [70,71]. We note that EPR studies at 9.5 GHz of these same highly C-doped GaN bulk substrate samples revealed an isotropic broad signal with a slightly

smaller g-value of 1.987 [72]. This difference with the g-values for the ODMR signals assigned to the two different charge states of C_N is puzzling and will be explored further.

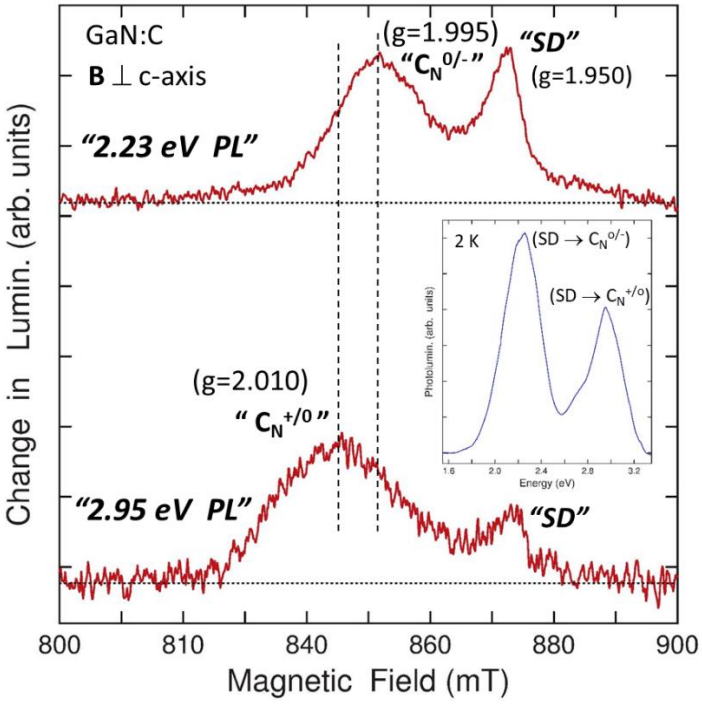

Figure 17. ODMR found at 24 GHz on the 2.23 eV (top spectrum) and 2.95 eV (bottom spectrum) broad PL bands from a GaN bulk sample with carbon doping level of 1×10^{18} cm^{-3}. A common feature labeled "SD" (shallow donor) and two unique resonances (as indicated by the dashed vertical lines) are revealed. Inset: PL observed at 2 K with 351 nm excitation.

4. Summary

For more than three decades, the need for semiconductor material systems able to operate at extreme conditions of voltage, current, and temperature have sent the material researchers on an intensive search for wide bandgap semiconductors that have the desired intrinsic physical and chemical properties. The wide bandgap semiconductor gallium nitride may be the best candidate to meet these needs. In spite of the lack of higher electronic grade native substrates, improved efficiency light emitters, solar-blind detectors, high-power solid-state switches and rectifiers, and high power, high frequency microwave transistors based on this material system have been commercialized. These devices exceed the performance of devices based on smaller band-gap semiconductors, and make possible new device designs. Despite this unprecedented and not fully developed semiconductor materials success, the realization of high-performance and high-yield devices will require native GaN substrates with well-controlled physical properties. Presently, Hydride Vapor Phase Epitaxy and Ammonothermal bulk growth are the only two methods that have successfully synthesized GaN bulk substrates. The acidic and basic ammonothermal methods are the only two growth approaches able to produce large area bulk single crystal GaN substrates from a small seed crystal. Wafers of both acidic and basic ammonothermal crystals have reduced dislocation densities and uniform lattice constants, consistent with very small X-ray full width diffraction peaks and bowing. Both types of crystals have high concentrations of oxygen, hydrogen, point defects, and complexes. These defects degrade the optical and electronic properties of ammonothermal GaN, seriously limiting the utilization of these wafers for the above mentioned devices. Ammonothermal GaN wafers have been successfully used as seeds to grow hydride vapor phase crystals with low dislocation density, and orders of magnitude lower concentration of unintended impurities, thus improving doping efficiency. Because epitaxial growth only reproduces the dimensions

of the substrate, larger ammonothermal substrates are required to produce larger HVPE GaN wafers. In this work, we illustrated the application of optical and paramagnetic techniques during various phases of GaN material growth using these two successful growth methods. The combination of these techniques has also allowed the identification of the chemical nature of pervasive impurities and the incorporation and activation of dopants, and the detrimental effect of extended defects on the distribution of free carriers.

Funding: This research did not received any external funding.

Data Availability Statement: All data have been previously reported in scientific journals.

Conflicts of Interest: The authors declare no conflict of interest.

References

1. Feigelson, B.N.; Frazier, R.M.; Freitas, J.A., Jr.; Fatemi, M.; Mastro, M.A.; Tischler, J.G. Seeded growth of GaN single crystals from solution at near atmospheric pressure. *J. Cryst. Growth* **2008**, *310*, 3934–3940. [CrossRef]
2. Yamane, H.; Shimada, M.; DiSalvo, F.J. Na flux growth and characterization of GaN single crystals. *Mater. Sci. Forum* **2000**, *325*, 21–24. [CrossRef]
3. Grezegory, I.; Bockowski, M.; Luznik, B.; Krukowski, K.; Romanowski, Z.; Wroblewski, M.; Porowski, S. Mechanism of crystallization of bulk GaN from solution under high N_3 pressure. *J. Cryst. Growth* **2002**, *246*, 177–186. [CrossRef]
4. Porowski, S.; Sadovyi, B.; Karbovnyk, I.; Gierlotka, S.; Rzoska, S.J.; Petrusha, I.; Stratiichuk, D.; Turkevich, V.; Grzegory, I. Melting of tetrahedrally bonded semiconductors: "anomaly" of the phase diagram of GaN. *J. Cryst. Growth* **2019**, *505*, 5–9. [CrossRef]
5. Yoshida, S.; Misawa, S.; Gonda, S. Improvements on the electrical and luminescent properties of reactive molecular beam epitaxially grown GaN films by using AlN-coated sapphire substrates. *Appl. Phys. Lett.* **1983**, *42*, 427. [CrossRef]
6. Amano, H.; Sawaki, N.; Akasaki, I.; Toyoda, T. Metalorganic vapor phase epitaxial growth of a high quality GaN film using an AlN buffer layer. *Appl. Phys. Lett.* **1986**, *48*, 353. [CrossRef]
7. Nakamura, S. Thermal Annealing Effects on P-Type Mg-Doped GaN Films. *Jpn. J. Appl. Phys.* **1992**, *31*, L139. [CrossRef]
8. Kamiyama, S.; Amano, H.; Akasaki, I. The Evolution of Nitrides Semiconductors. In *Optoeletronics Devices: III-Nitrides*; Razighi, M., Henini, M., Eds.; Elsevier Ltd.: Amsterdam, The Netherlands, 2004; pp. 23–38.
9. Bergman, L.; Dutta, M.; Nemanich, R.J. *Raman Scattering in Materials Science*; Springer Series in Material Science; Weber, W.H., Merlin, R., Eds.; Springer: Berlin/Heidelberg, Germany, 2000; Volume 42, p. 273.
10. Maruska, H.P.; Tietjen, J.J. The preparation and properties of vapor-deposited single-crystal-line GaN. *Appl. Phys. Lett.* **1969**, *15*, 327. [CrossRef]
11. Kelly, M.K.; Vaudo, R.P.; Phance, V.M.; Gögens, L.; Ambacher, O.; Stutzmanm, M. Large Free-Standing GaN Substrates by Hydride Vapor Phase Epitaxy and Laser-Induced Liftoff. *Jpn. J. Appl. Phys.* **1999**, *38*, L217. [CrossRef]
12. Park, S.S.; Park, I.-W.; Choh, S.H. Free-Standing GaN Substrates by Hydride Vapor Phase Epitaxy. *Jpn. J. Appl. Phys.* **2000**, *39*, L1141–L1142. [CrossRef]
13. Paskova, T.; Darakchieva, V.; Paskov, P.P.; Söderwall, U.; Monemar, B. Growth and separation related properties of HVPE-GaN free-standing films. *J. Cryst. Growth* **2002**, *246*, 207. [CrossRef]
14. Yoshida, T.; Oshima, Y.; Eri, T.; Ikeda, K.; Yamamoto, S.; Watanabe, K.; Shibata, M.; Mishima, T.J. Fabrication of 3-in GaN substrates by hydride vapor phase epitaxy using void-assisted separation method. *J. Cryst. Growth* **2008**, *310*, 5–7. [CrossRef]
15. Hanser, D.; Tudor, M.; Preble, E.A.; Williams, M.; Xu, X.; Tsvetkov, D.; Liu, L. Surface preparation of substrates from bulk GaN crystals. *J. Cryst. Growth* **2007**, *305*, 372. [CrossRef]
16. Freitas, J.A., Jr.; Gowda, M.; Tischler, J.G.; Kim, J.-H.; Liu, L.; Hanser, D. Semi-insulating GaN substrates for high-frequency device fabrication. *J. Cryst. Growth* **2008**, *310*, 3968. [CrossRef]
17. Ballman, A.A.; Dodd, D.M.; Kuebler, N.A.; Laudise, R.A.; Wood, D.L.; Rudd, D.W. Synthetic quartz with high ultraviolet transmission. *Appl. Opt.* **1968**, *7*, 1387. [CrossRef]
18. Ehrentrautt, D.; Bockowski, M. Bulk crystal growth: Basic techniques, and growth mechanisms and dynamics. In *Handbook of Crystal Growth*, 2nd ed.; Rudoph, P., Ed.; Elsevier: Amsterdam, The Netherlands, 2015; pp. 577–619.
19. Doradzinski, R.; Dwillinski, R.; Garcznski, J.; Sierzputowski, L.P.; Kanbara, Y. *Technology of Gallium Nitride Crystal Growth*; Ehrentraut, D., Meissiner, E., Bockowski, M., Eds.; Spring-Verlag: Berlin/Heidelberg, Germany, 2010; pp. 137–158.
20. Wang, B.; Callahan, M.J. Ammonothermal Synthesis of III-Nitride Crystals. *Cryst. Des.* **2006**, *6*, 1227. [CrossRef]
21. Dwillinski, R.; Doradzinski, R.; Garcznski, J.; Sierzputowski, L.P.; Kucharski, R.; Rudzinski, M.; Zajac, M.; Kudrawiec, R. Properties of truly bulk GaN monocrystals grown by ammonothermal method. *Phys. Status Solid C* **2009**, *6*, 2661. [CrossRef]
22. Sochacki, T.; Amilusiki, M.; Lucznik, B.; Fijalkowski, M.; Weyhar, J.L.; Sadovyi, B.; Kamler, G.; Nowak, G.; Litwin-Staszewska, E.; Khachapuridze, A.; et al. Preparation of free-standing GaN substrates from GaN layers crystallized by hydride vapor phase epitaxy on ammonothermal GaN seeds. *Jpn. J. Appl. Phys.* **2014**, *53*, 05FA04. [CrossRef]
23. Freitas, J.A., Jr.; Culbertson, J.C.; Mahadik, N.A.; Sochacki, T.; Bockowski, M.; Iwinska, M. Growth of high crystalline quality HVPE-GaN crystals with controlled electrical properties. *Cryst. Growth Des.* **2015**, *15*, 4837. [CrossRef]

24. Kozawa, T.; Kachi, T.; Kano, H.; Nagase, H.; Koide, N.; Manabe, K. Thermal stress in GaN epitaxial layers grown on sapphire substrates. *J. Appl. Phys.* **1995**, *77*, 4389. [CrossRef]
25. Freitas, J.A., Jr.; Culbertson, J.C.; Mahadik, N.A.; Glaser, E.R.; Sochccki, T.; Bockowski, M. Incorporation of pervasive impurities on HVPOE GaN growth directions. *J. Cryst. Growth* **2016**, *456*, 101–107. [CrossRef]
26. Gogova, D.; Petrov, P.P.; Buegler, M.; Wagner, M.R.; Nestiel, C.; Callsen, G.; Schmidbauert, M.; Kucharski, R.; Zajac, M.; Dwilinski, R.; et al. Structural and optical investigation of non-polar (1–100) GaN grown by the ammonothermal method. *J. Appl. Phys.* **2013**, *113*, 203513. [CrossRef]
27. Perlin, P.; Camassel, J.; Knap, W.; Talercio, T.; Chervin, J.C.; Suski, T.; Grzegory, I.; Porowski, S. Investigation of longitudinal-optical phonon-plasmon coupled modes in highly conducting bulk GaN. *Appl. Phys. Lett.* **1995**, *67*, 2524. [CrossRef]
28. Kim, H.-Y.; Freitas, J.A., Jr.; Kim, J. Penetration Effects of High-Energy Protons in GaN: A Micro-Raman Spectroscopy Study. *Electrochem. Sol.-St. Lett.* **2011**, *14*, H5–H8. [CrossRef]
29. Freitas, J.A., Jr.; Zajac, M. Chapter 16, Properties of Ammonthermal Crystals. In *Ammonothermal Synthesis and Crystal Growth of Nitrides*; Spring Series in Materials Science; Maissener, E., Niewa, R., Eds.; Springer: Cham, Switzerland, 2021; Volume 304, pp. 287–314.
30. Zając, M.; Kucharski, R.; Grabianska, K.; Gwardys-Bak, A.; Puchalski, A.; Domagala, J.Z.; Piotrzkowski, R.; Litwin-Staszewska, E.; Wasik, D.; Bockowski, M. Basic ammonothermal growth of Gallium Nitride—State of the art, challenges, perspectives. *Prog. Cryst. Growth Charact. Mat.* **2018**, *64*, 63. [CrossRef]
31. Freitas, J.A., Jr.; Culbertson, J.C.; Mahadik, N.A.; Sochacki, T.; Bockowski, M. HVPE GaN wafers with improved crystalline and electrical properties. *J. Cryst. Growth* **2016**, *456*, 113. [CrossRef]
32. Freitas, J.A., Jr.; Khan, M.A. Raman and Photoluminescence Studies of Undoped and Magnesium-Doped Gan Films on Sapphire. *Mat. Res. Soc.* **1994**, *339*, 547. [CrossRef]
33. Ogino, T.; Aoki, M. Mechanism of yellow luminescence in GaN. *Jpn. J. Appl. Phys.* **1980**, *19*, 2395–2405. [CrossRef]
34. Freitas, J.A., Jr.; Braga, G.C.B.; Moore, W.J.; Tischler, J.G.; Culbertson, J.C.; Fatemi, M.; Park, S.S.; Lee, S.K.; Park, Y. Structural and optical properties of thick freestanding GaN templates. *Cryst. Growth* **2001**, *231*, 322–328. [CrossRef]
35. Freitas, J.A., Jr.; Tischler, J.G.; Garces, N.Y.; Feigelson, B.N. Optical probing of low-pressure solution growth GaN crystal properties. *J. Cryst. Growth* **2010**, *312*, 2564–2568. [CrossRef]
36. Freitas, J.A., Jr.; Moore, W.J.; Shanabrook, B.V.; Braga, G.C.B.; Lee, S.K.; Park, S.S.; Han, J.Y. Donor-related recombination processes in hydride-vapor-phase epitaxial GaN. *Phys. Rev. B* **2002**, *66*, 233311. [CrossRef]
37. Moore, W.J.; Freitas, J.A., Jr.; Braga, G.C.B.; Molnar, R.J.; Lee, S.K.; Lee, K.Y.; Song, I.J. Identification of Si and O donors in hydride-vapor-phase epitaxial GaN. *Appl. Phys. Lett.* **2001**, *79*, 2570. [CrossRef]
38. Gil, B.; Bigenwald, P.; Paskov, P.P.; Monemar, B. Internal structure of acceptor-bound excitons in wide-band-gap wurtzite semiconductors. *Phys. Rev. B* **2010**, *81*, 085211. [CrossRef]
39. Moore, W.J.; Freitas, J.A., Jr.; Lee, S.K.; Park, S.S.; Han, J.Y. Magneto-optical studies of free-standing hydride-vapor-phase epitaxial GaN. *Phys. Rev. B* **2002**, *65*, 081201. [CrossRef]
40. Ilegems, M.; Dingle, R.; Logan, R.A. Luminescence of Zn-and Cd-doped GaN. *J. Appl. Phys.* **1972**, *43*, 3797. [CrossRef]
41. Xing, H.; Green, D.S.; Yu, H.; Mates, T.; Kozodoy, P.; Keller, S.; DenBaars, S.P.; Mishra, U.K. Memory Effects and Redistribution of Mg into Sequentially Regrown Chemical Vapor Deposition. *Jpn. J. Appl. Phys.* **2003**, *42*, 50. [CrossRef]
42. Freitas, J.A., Jr.; Feigelson, B.N.; Anderson, T.J. Efficient incorporation of Mg in solution grown GaN crystals. *Appl. Phys. Express* **2013**, *6*, 111001.
43. Freitas, J.A., Jr.; Culbertson, J.C.; Mahadik, N.A.; Tadjer, M.J.; Wu, S.; Raghothamachar, B.; Dudley, M.; Sochacki, T.; Bockowski, M. Homoepitaxial HVPE GaN: A potential substrate for high performance devices. *J. Cryst. Growth* **2018**, *500*, 104. [CrossRef]
44. Freitas, J.A., Jr.; Moore, W.J.; Shanabrook, B.V.; Braga, G.C.B.; Koleske, D.D.; Lee, S.K.; Park, S.S.; Han, J.Y. Shallow donors in GaN. *Phys. Stat. Sol.* **2003**, *240*, 330. [CrossRef]
45. Fujikura, H.; Yoshida, T.; Shibata, M.; Otoki, Y. Recent progress of high-quality GaN substrates by HVPE method. In Proceedings of the Gallium Nitride Materials and Devices XII, SPIE OPTO, San Francisco, CA, USA, 28 January–2 February 2017; Volume 10104, p. 1010403.
46. Kang, B.S.; Ren, F.; Irokawa, Y.; Baik, K.W.; Pearton, S.J.; Pan, C.-C.; Chen, G.-T.; Chyi, J.-I.; Ko, H.-J.; Lee, H.-Y. Temperature dependent characteristics of bulk GaN Schottky rectifiers on free-standing GaN substrates. *J. Vac. Sci. Technol. B Microelectron. Process. Phenom.* **2004**, *22*, 710. [CrossRef]
47. Heitz, R.; Maxim, P.; Eckey, L.; Thurian, P.; Hoffmann, A.; Broser, I.; Pressal, K.; Meyer, B.K. Excited states of Fe^{3+} in GaN. *Phys. Rev. B* **1997**, *55*, 4382. [CrossRef]
48. Iwinska, M.; Piotrzkowski, R.; Litwin-Staszewska, E.; Sochacki, T.; Amilusik, M.; Fijalkowski, M.; Lucznik, B.; Bockowski, M. Highly resistive C-doped hydride vapor phase epitaxy-GaN grown on ammonothermally crystallized GaN seeds. *Appl. Phys. Express* **2017**, *10*, 011003. [CrossRef]
49. Freitas, J.A., Jr.; Tischler, J.G.; Kim, J.-H.; Kumagai, Y.; Koukitu, A. Properties of Fe-doped semi-insulating GaN substrates for high-frequency device fabrication. *J. Cryst. Growth* **2007**, *305*, 403–407. [CrossRef]
50. Talut, G.; Reuther, H.; Mücklich, A.; Eichhorn, F.; Potzger, K. Nanocluster formation in Fe implanted GaN. *Appl. Phys. Lett.* **2006**, *89*, 161909. [CrossRef]

51. Iwinska, M.; Piotrzkowski, R.; Litwin-Staszewska, E.; Ivanov, V.Y.; Teisseyre, H.; Amilusik, M.; Lucznik, B.; Fijalkowski, M.; Sochacki, T.; Takekawa, N.; et al. Crystallization of semi-insulating HVPE-GaN with solid iron as a source of dopants. *J. Cryst. Growth* **2017**, *475*, 121. [CrossRef]
52. Freitas, J.A., Jr.; Culbertson, J.C.; Glaser, E.R.; Richter, E.; Weyers, M.; Oliveira, A.C.; Garg, V.K. Efficient iron doping of HVPE GaN. *J. Cryst. Growth* **2018**, *500*, 111–116. [CrossRef]
53. Malguth, E.; Hoffman, A.; Gehlhoff, W.; Gelhausen, O.; Phillips, M.R.; Xu, X. Strutural and electronic properties of Fe^{3+} and Fe^{2+} centers in GaN from optical and EPR experiments. *Phys. Rev. B* **2006**, *74*, 125202. [CrossRef]
54. Freitas, J.A., Jr.; Mastro, M.A.; Glaser, E.R.; Garces, N.Y.; Lee, S.K.; Chung, J.H.; Oh, D.K.; Shim, K.B. Structural and optical studies of thick freestanding GaN films deposited by hydride vapor phase epitiaxy. *J. Cryst. Growth* **2012**, *350*, 27–32. [CrossRef]
55. Carlos, W.E.; Freitas, J.A., Jr.; Khan, M.A.; Olson, D.T.; Kuznia, J.N. Electron-spin-resonance studies of donors in wurtzite GaN. *Phys. Rev. B* **1993**, *48*, 17878–17884. [CrossRef]
56. Reinacher, N.M.; Angerer, H.; Ambacher, O.; Brandt, M.S.; Stutzmann, M. Spin resonance investigations of GaN and AlGaN. *Mat. Res. Soc. Symp. Proc.* **1997**, *449*, 579–584. [CrossRef]
57. Palczewska, M.; Suchanek, B.; Dwilinksi, R.; Pakula, K.; Wagner, A.; Kaminska, M. Paramagnetic defects in GaN. *MRS Internet J. Nitride Semicond. Res.* **1998**, *3*, 45. [CrossRef]
58. Maier, K.; Kunzer, M.; Kaufmann, U.; Schneider, J.; Monemar, B.; Akasaki, I.; Amano, H. Iron acceptors in gallium nitride (GaN). *Mater. Sci. Forum* **1994**, *143–147*, 93–98. [CrossRef]
59. Gelhoff, W.; Azamat, D.; Haboeck, U.; Hoffmann, A. Preferential substitution of Fe on physically equivalent Ga sites in GaN. *Physica B* **2006**, *376–377*, 486–490. [CrossRef]
60. Glaser, E.R.; Freitas, J.A., Jr.; Reshchikov, M.A.; Zvanut, M.E.; Leach, J.H.; Udwary, K. Optical and Magnetic Resonance Studies of Mg-doped GaN Bulk Substrates grown by Hydride Vapor Phase Epitaxy. Unpublished work. 2022.
61. Zvanut, M.E.; Dashdorj, J.; Freitas, J.A., Jr.; Glaser, E.R.; Willoughby, W.; Leach, J.H.; Udwary, K. Incorporation of Mg in free-standing HVPE GaN substrates. *J. Electron. Mater.* **2016**, *45*, 2692–2696. [CrossRef]
62. Malyshev, A.V.; Merkulov, I.A.; Rodina, A.V. Ground state characteristics of an acceptor center in wide-bandgap semiconductors with a weak spin-orbit coupling. *Phys. Solid State* **1998**, *40*, 917–923. [CrossRef]
63. Glaser, E.R.; Murthy, M.; Freitas, J.A., Jr.; Storm, D.F.; Zhou, L.; Smith, D.J. Optical and magnetic resonance studies of Mg-doped GaN homoepitaxial layers grown by molecular beam epitaxy. *Physica B* **2007**, *401–402*, 327–330. [CrossRef]
64. Glaser, E.R.; Carlos, W.E.; Braga, G.C.B.; Freitas, J.A., Jr.; Moore, W.J.; Shanabrook, B.V.; Henry, R.L.; Wickenden, A.E.; Koleske, D.D.; Obloh, H.; et al. Magnetic resonance studies of Mg-doped GaN epitaxial layers grown by organometallic chemical vapor deposition. *Phys. Rev. B* **2002**, *65*, 085312. [CrossRef]
65. Lyons John, L.; Glaser Evan, R.; Zvanut, M.E.; Paudel, S.; Iwinska, M.; Sochacki, T.; Bockowski, M. Carbon complexes in highly C-doped GaN. *Phys. Rev. B* **2021**, *104*, 075201. [CrossRef]
66. Glaser, E.R.; Kennedy, T.A.; Doverspike, K.; Rowland, L.B.; Gaskill, D.K.; Freitas, J.A.; Asif Khan, M.; Olson, D.T.; Kuznia, J.N.; Wickenden, D.K. Optically detected magnetic resonance of GaN films grown by organometallic chemical vapor deposition. *Phys. Rev. B* **1995**, *51*, 13326–13336. [CrossRef]
67. Kaufmann, U.; Kunzer, M.; Merz, C.; Akasaki, I.; Amano, H. Light generating carrier recombination and impurities in wurtzite GaN/Al_2O_3 grown by MOCVD. *Mater. Res. Soc. Symp. Proc.* **1996**, *395*, 633–643. [CrossRef]
68. Koschnick, F.K.; Michael, K.; Spaeth, J.-M.; Beaumont, B.; Gibart, P. Optical detection of electron nuclear double resonance on a residual shallow donor in wurtzite GaN. *Phys. Rev. B* **1996**, *54*, R11042–R11045. [CrossRef] [PubMed]
69. Mason, P.W.; Dörnen, A.; Haerle, V.; Scholz, F.; Watkins, G.D. Yellow luminescence and associated ODMR in OMVPE GaN: A comparison of defect models. *Mater. Res. Soc. Symp. Proc.* **1997**, *449*, 793–798. [CrossRef]
70. Lyons, J.L.; Janotti, A.; Van de Walle, C.G. Effects of carbon on the electrical and optical properties of InN, GaN, and AlN. *Phys. Rev. B* **2014**, *89*, 035204. [CrossRef]
71. Reshchikov, M.A.; Vorobiov, M.; Demchenko, D.O.; Özgür, U.; Morkoç, H.; Lesnik, A.; Hoffmann, M.P.; Hörich, F.; Dadgar, A.; Strittmatter, A. Two charge states of the C_N acceptor in GaN: Evidence from photoluminescence. *Phys. Rev. B* **2018**, *98*, 125207. [CrossRef]
72. Zvanut, M.E.; Paudel, S.; Sunay, U.R.; Willoughby, W.R.; Iwinska, M.; Sochacki, T.; Bockowski, M. Charge transfer process for carbon-related center in semi-insulating carbon-doped GaN. *J. Appl. Phys.* **2018**, *124*, 075701. [CrossRef]